frontiers in Physics

TYPE Original Research
PUBLISHED 24 July 2026
DOI 10.3389/fphy.2026.1819239

Check for updates

OPEN ACCESS

EDITED BY
Ivo Rausch,
Medical University of Vienna, Austria

REVIEWED BY
Shlair Ibrahim,
University of Kirkuk College of Medicine, Iraq
Aytaç Levet,
Atatürk Üniversitesi, Türkiye

*CORRESPONDENCE
Heba Alrakh,
h.alrakh@fz-juelich.de

RECEIVED 27 February 2026
REVISED 21 June 2026
ACCEPTED 23 June 2026
PUBLISHED 24 July 2026

CITATION
Alrakh H, Tellmann L, Nikoubashman O, Zimmermann M, Shokrgozar S, Winz OH, Faby S, Abu arra A, Wiesmann M, Shah NJ and Lerche C (2026) Comparison of PET photon attenuation for human tissue compositions, tissue-equivalent material compositions, and CT-phantom measurements. *Front. Phys.* 14:1819239. doi: 10.3389/fphy.2026.1819239

COPYRIGHT
© 2026 Alrakh, Tellmann, Nikoubashman, Zimmermann, Shokrgozar, Winz, Faby, Abu arra, Wiesmann, Shah and Lerche. This is an open-access article distributed under the terms of the Creative Commons Attribution License (CC BY). The use, distribution or reproduction in other forums is permitted, provided the original author(s) and the copyright owner(s) are credited and that the original publication in this journal is cited, in accordance with accepted academic practice. No use, distribution or reproduction is permitted which does not comply with these terms.

Comparison of PET photon attenuation for human tissue compositions, tissue-equivalent material compositions, and CT-phantom measurements

Heba Alrakh[1,2]*, Lutz Tellmann[1], Omid Nikoubashman[3], Maike Zimmermann[3], Sadaf Shokrgozar[3], Oliver H. Winz[4], Sebastian Faby[5], Ali Abu arra[6], Martin Wiesmann[3], N. Jon Shah[1,2,7,8] and Christoph Lerche[1]

[1]INM-4, Forschungszentrum Jülich GmbH, Jülich, Germany, [2]Department of Neurology, RWTH Aachen University, Aachen, Germany, [3]Department of Diagnostic and Interventional Neuroradiology, RWTH Aachen University, Aachen, Germany, [4]Department of Nuclear Medicine, University Hospital RWTH Aachen, Aachen, Germany, [5]Department of Computed Tomography, Siemens Healthineers AG, Forchheim, Germany, [6]Department of Biophysics and Medical Imaging, An-Najah National University, Nablus, Palestine, [7]INM-11, Forschungszentrum Jülich GmbH, Jülich, Germany, [8]JARA - BRAIN - Translational Medicine, Aachen, Germany

Introduction: In this study, the accuracy of linear attenuation coefficients for annihilation photons (511 keV) and additional cascade gammas (603, 1,077, and 1,157 keV) derived from two commercially available phantoms, i.e., the Sun Nuclear electron density and DIAGNOMATIC Pro-RT ED phantoms, was evaluated.

Methods: LACs obtained from computations using the NIST XCOM database and literature values of real tissue compositions were compared to LACs obtained from computations using the NIST XCOM database and tissue-equivalent inserts (when available) and to LACs obtained from transmission measurements. Also, LACs obtained from computations using the NIST XCOM database and tissue-equivalent inserts were compared to LACs obtained from transmission measurements (when possible). In addition, transmission scans were performed using the ECAT EXACT HR + positron emission tomography scanner.

Results: Twelve out of 23 tissue-equivalent inserts showed a deviation in the LACs of less than 5% when the values obtained from transmission measurements were compared to those computed using the NIST XCOM database with literature values of real tissue compositions. The highest relative errors were observed in lung-equivalent tissues (up to 37.45) and solid dense bone inserts (26.10%).

Discussion: Combining the breast and solid trabecular bone inserts of the Diagnomatic Pro-RT ED phantom with the liver, brain, adipose, lung-450, inner bone, cortical bone, HE Blood 40, HE Blood 70 and HE Blood 100 inserts from the Sun Nuclear phantom provides a relatively complete set of tissue-equivalent inserts from CT phantoms that reproduce the attenuation with systematic errors below 5%.

KEYWORDS

attenuation coefficients, attenuation correction, phantom material composition, tissue composition, transmission scan

1 Introduction

Quantitative positron emission tomography (PET) requires accurate attenuation correction (AC) to account for the photon loss due to interactions with matter. This requires precise knowledge of the linear attenuation coefficients μ (LACs) at 511keV, yet the ground-truth values for real tissue LACs cannot be determined *in vivo*.

In CT-based attenuation correction, and in some MR-based approaches, attenuation maps are typically derived from CT images by converting Hounsfield Units (HUs) to LACs at 511 keV. Carney et al. [1] proposed a conversion scheme based on measurements with the Gammex 467 electron density CT phantom (GAMMEX RMI, Middleton, Wisconsin), where literature values of real tissue compositions were used to define the corresponding LACs at 511 keV. However, CT uses a poly-energetic X-ray beam, while PET γ-photons are mono-energetic, complicating these conversions [2]. A calculation with simulated CT spectra for 120 kV tube voltage showed that the difference between the average attenuation obtained from a poly-energetic spectrum and the attenuation obtained at the average CT energy of a mono-energetic spectrum can reach up to 30% when different materials are considered (in the case of a phantom insert enriched with calcium). This error propagates into the extrapolation scheme to 511 keV and higher energies. Xia et al. [3] reported generally smaller biases for the mono-energetic spectrum compared to the poly-energetic spectrum, where the bias in the latter case can reach up to 11%. Spectral CT techniques, such as dual-energy or photon-counting CT, allow for material decomposition [4] and the computation of virtual mono-energetic images, potentially offering a solution to this problem and improving extrapolation of LACs from poly-energetic energies in the CT energy range to 511 keV. Before the advent of combined PET/CT imaging, transmission scans with radioactive sources, e.g., $^{68}Ga/^{68}Ge$ or ^{137}Cs were used. Although these transmission scans allow the measurement of mono-energetic attenuation coefficients, these measurements are also subjected to systematic errors resulting from no or only approximate scatter correction, reconstruction artefacts, and other effects. Consequently, systematic deviations of the LACs from the real values are present in any existing method.

In PET/MR systems, attenuation correction is even more challenging due to the lack of a direct relationship between the MR signal and the spin interactions of the protons and electron density relevant for the attenuation. Various methods have been proposed for MR-based AC, including atlas- and template-based methods, and more recently, machine learning models [5–8]. A comparison was conducted between three MR-based attenuation correction methods, focusing on the cerebellum, to evaluate the performance of atlas- and template-based approaches relative to a CT-based method [2].

Phantom-based LAC measurements allow for the determination of LACs in the phantom material and have the advantage that the ground truth, i.e., the material's attenuation properties, is more precisely known than for living tissue. Although they are highly reproducible when identical scanner configurations are used, they introduce another uncertainty, as they normally only mimic the behaviour of real tissues for a single imaging modality, such as CT or PET. However, direct *in vivo* measurements is not practical as it would expose subjects to ionising radiation. In addition, it should be noted that *in vivo* measurements are also subject to natural biological inner and intra-subject variations [9–11]. These variations can be physiological, such as ageing, physical activity, and nutrition, or pathological, such as obesity, osteoporosis, etc. These variations can result in changes in density and the effective atomic number, Z_{eff}, of up to a few percentage points [12]. Here, it should also be noted that the photoelectric cross section, which is dominant for CT energies, is proportional to the 3-4 power of Z_{eff}, whereas the Compton cross section, which is dominant for PET energies, is proportional to Z_{eff} [13]. Therefore, the composition of a phantom must closely approximate its biological tissue, within the level of accuracy required for the intended application, including the energy range of the used radiation. According to Report 44 of the International Commission on Radiation Units and Measurements [14], tissue-equivalent materials should have LACs within ±5% of those of human tissue over the relevant photon energy range.

The determination of real LACs is very difficult due to systematic differences between living and *postmortem* tissue, and because any indirect measurement may also suffer from conversion errors. Singh et al. studied the radiation interaction properties of tissue equivalent materials for cortical bone, muscle tissue, and lung tissue over a wide range of photon energies, specifically at 60, 81, 112, 184, 356, 511, 662, 834, and 1120 keV [15]. A comparison was subsequently performed between the calculated total mass attenuation coefficients (μ/ρ) of the tissue substitutes and those of the corresponding real tissue, where ρ is the mass density. In addition, they used measured back-scatter intensities to compare computed effective atomic numbers, Z_{eff}, to the corresponding values determined from these measurements for different materials. Their findings underscore the significant variations in radiation response between different tissues, with cortical bone exhibiting the highest photon attenuation, as expected. The results obtained by Singh et al. are particularly relevant to the current research and will serve as a reference point for comparison. A detailed discussion will be presented in the discussion section of this paper.

Important work on radiation dosimetry and imaging was conducted by White in 1978 [16], who conducted a comprehensive review of tissue substitutes used in experimental radiation physics. The study analysed the chemical composition, physical density, and radiological properties (including photon and electron interaction characteristics) of 64 materials designed to mimic human tissues. These materials were evaluated for their suitability as tissue-equivalent substitutes in phantom construction. This work provided detailed guidance on material selection for simulating realistic human anatomy in both therapeutic and diagnostic settings.

The NIST XCOM database is a widely used resource that provides photon cross sections for coherent and incoherent scattering, photoelectric absorption, and pair production, as well as total attenuation coefficients, for elements, compounds, and mixtures over an energy range from 1keV to 100 GeV [17]. This web-based tool enables precise calculations, essential for modeling radiation transport in both clinical and research contexts. The total photon cross section is the combination of incoherent (Compton) and coherent (Rayleigh) scattering, photoelectric absorption, and pair production mass attenuation coefficients; detailed methodologies for calculating each interaction process are provided in the NIST XCOM Photon Cross Sections

Database. Interaction and total attenuation coefficients are used for the computation according to XCOM. For compounds, values are obtained as weighted sums over the corresponding coefficients for elements. Weight factors are automatically computed using the fractions by weights of the atomic constituents obtained from the chemical formula provided by the user. Ermis et al. provided a detailed investigation into mass attenuation coefficients of blood, bone, lung, eye lens, adipose tissue, muscle, brain, and skin using theoretical methods such as FLUKA, GEANT4 Monte Carlo simulations, and the XCOM program [18].

Only a limited number of further studies have investigated the attenuation properties of tissue-equivalent materials. Frimaio et al. [19] developed four resin-based water-equivalent materials and established a methodology to measure their LACs at energies of 60, 80, 100, and 120 kV. Nascimento et al. [20] extended this work to a broader diagnostic energy range (5–150 keV). Kabir et al. [21] investigated attenuation coefficients at average energies of 16.61, 17.47, 21.17, and 25.26keV, CT numbers at 120 kV, chemical composition, and the electron density of a breast phantom. Gokcekuyu et al. [22] compared real tissues and tissue-equivalent materials using a dental phantom. Geraldelli et al. [23] measured transmitted and scattered X-rays to characterise the attenuation and scattering properties of seven tissue-equivalent materials over photon energy ranging from 10 to 60 keV. Also, different studies have investigated the radiological features for different materials, such as mass attenuation coefficient, effective atomic number, half value layer, and mean free path for low-energy photons, i.e., photons with energy between 0.1 and 10 keV [24, 25].

Amin et al. [26] determined the mass attenuation coefficients of two mixtures of paraffin wax and NaCl, which were designed to simulate soft tissue and bone tissue, over the energy range of 60keV to 1.33 MeV. The measured values were compared with those obtained using semi-empirical relations based on the mixture rule, values from the XCOM, and the ICRU report 44.

To the best of our knowledge, only the study conducted by Singh et al. [15] investigated the attenuation properties of the tissue-equivalent materials at the photon energy relevant to positron emission tomography (511 keV); however, the work focused primarily on estimating the effective atomic number and other interaction parameters (e.g., kerma, fluence, and dose) to evaluate radiation risk in human tissues, and CT phantoms were not used in the study. Moreover, their approach was based on saturation thickness measurement and was limited to a small number of tissues (cortical bone, muscle, and lung). Consequently, it did not address discrepancies in obtaining 511 keV LACs from different methods.

The ICRU Report 44 states that tissue-equivalent materials should exhibit LACs within ±5% when compared to those of human tissues over the relevant photon energy range. However, the systematic difference in attenuation between real tissue and tissue substitute depends on the specific composition of the material used to emulate the tissue. In this work, we aim to quantify these differences. In addition, we compare the results with transmission measurements and consider other γ-photons energies, including those of ^{124}I, ^{68}Ga, and ^{44}Sc. Interest in these radionuclides has recently increased in the context of multiplexed PET imaging [27–29], and correct attenuation correction at these energies is essential for quantitatively accurate reconstruction [30]. Our main focus will be on tissues present in the head, as the results from this work shall be used for improved attenuation map generation for brain imaging.

2 Materials and methods

The Sun Nuclear electron density phantom and the DIAGNOMATIC Pro-RT ED phantom were used to investigate the attenuation properties of their materials, which were then compared with literature values of corresponding real tissues, enabling a detailed assessment of radiological equivalence at the energy level used in PET imaging.

2.1 Materials

2.1.1 Phantoms

The Sun Nuclear electron density phantom enables tissue-equivalent CT value to electron density calibration. The inserts are manufactured to meet medical standards for human tissue densities in accordance with ICRU-44 and ICRP specifications. The in-plane dimensions of the phantom are 40 cm*30 cm, and it has a removable head section with a 20 cm diameter, which was the only part used in this study. The phantom has several inserts, but for our study, only the following interchangeable inserts were used: lung LN-300, lung LN-450, adipose, breast, liver, brain, true water, inner bone, cortical bone, 50% $CaCO_3$, three blood-mimicking materials at relative electron densities of 1.03, 1.07, and 1.10, and two blood-mimicking materials plus iodine at 2and 4 mg/mL. The diameter of each insert is 28.6 mm. The physical densities and chemical compositions of the inserts are shown in Table 1. These were later utilised to determine the LACs of the tissue-equivalent inserts.

The DIAGNOMATIC Pro-RT ED phantom is designed to represent tissue heterogeneity in radiotherapy treatment planning with CT. Its dimensions are 33 cm*27 cm*5 cm, and it has a removable head section with a diameter of 18 cm, which was the only part used in our study. The phantom includes inserts emulating the following tissues: lung (inhale), lung (exhale), breast, solid trabecular bone 200 mg/cc HA, liver, muscle, adipose tissue, solid dense bone 800 mg/cc HA, and solid dense bone 1250 mg/cc HA, together with a water-filled insert. The physical densities of the inserts are shown for completeness in Table 2, as provided in the phantom data sheet; however, they were not utilised in subsequent analysis, as the chemical compositions were not provided by the manufacturer, and consequently, the LACs could not be determined for these insert materials.

2.1.2 Scanners

Two scanners were used to compare the LACs at 511 keV obtained with different methods. Transmission scans were performed using the ECAT EXACT HR + scanner [31] and reconstructed using a 2D OSEM algorithm with six iterations and 16 subsets, with 4 mm gaussian filter; scatter correction was applied during the measurements. The Siemens Healthineers NAEOTOM Alpha photon-counting CT (PCCT) scanner [32] was also used to

TABLE 1 Physical density (g/cm^3) and chemical composition of the used inserts of the Sun Nuclear electron density phantom.

Inserts	H	B	C	N	O	Others	ρ (g/cm^3)
Liver	8.25	0.03	66.87	2.25	19.02	0.10 Na, 0.75 Mg, 0.65 Si, 0.14 Cl, 1.94 Ca	1.08
Brain	8.23	0.04	65.75	2.05	19.70	0.15 Na, 1.23 Mg, 0.94 Si, 0.13 Cl, 1.79 Ca	1.05
Breast	9.48	0.04	70.23	2.47	15.13	0.16 Na, 0.61 Mg, 1.01 Si, 0.12 Cl, 0.74 Ca	0.98
Adipose	9.73	0.05	71.41	2.71	14.35	0.18 Na, 1.11 Si, 0.12 Cl, 0.34 Ca	0.96
Lung LN-300	7.43		57.86	1.96	20.71	11.19 Mg, 0.77 Si, 0.08 Cl	0.29
Lung LN-450	7.44		58.03	1.97	20.69	11.22 Mg, 0.57 Si, 0.08 Cl	0.45
Inner bone	6.38	0.03	53.79	1.73	25.64	0.11 Na, 1.68 Mg, 0.72 Si, 0.10 Cl, 9.82 Ca	1.21
Cortical bone	2.31		27.41	0.85	39.95	2.82 Mg, 0.04 Cl, 26.62 Ca	1.93
50% $CaCO_3$	4.03		40.34	1.52	34.13	0.30 Mg, 0.07 Cl, 19.62 Ca	1.56
HE blood 40	8.37	0.03	66.85	2.16	18.59	0.13 Na, 1.11 Mg, 0.79 Si, 0.13 Cl, 1.74 Ca, 0.10 Fe	1.06
HE blood 70	8.44	0.02	67.42	2.18	18.35	0.08 Na, 1.11 Mg, 0.49 Si, 0.14 Cl, 1.67 Ca, 0.10 Fe	1.095
HE blood 100	8.50	0.01	67.96	2.20	18.12	0.03 Na, 1.11 Mg, 0.22 Si, 0.14 Cl, 1.61 Ca, 0.10 Fe	1.13
Blood 40 + 2 mg/mL Iod	8.36	0.03	66.75	2.15	18.53	0.12 Na, 1.11 Mg, 0.78 Si, 0.13 Cl, 1.73 Ca, 0.10 Fe, 0.19 I	1.061
Blood 40 + 4 mg/mL Iod	8.34	0.03	66.65	2.15	18.47	0.12 Na, 1.10 Mg, 0.78 Si, 0.13 Cl, 1.73 Ca, 0.10 Fe, 0.39 I	1.063

TABLE 2 The DIAGNOMATIC Pro-RT ED phantom mass density (g/cm^3).

Inserts	ρ (g/cm^3 $\pm$%)
Liver	1.075$\pm$1
Breast	0.985$\pm$1
Muscle	1.055$\pm$1
Adipose tissue	0.935$\pm$1
Lung (inhale)	0.175$\pm$9
Lung (exhale)	0.67$\pm$1.5
Solid trabecular bone 200 mg/cc HA	1.18$\pm$2
Solid dense bone 800 mg/cc HA	1.42$\pm$1
Solid dense bone 1250 mg/cc HA	1.56$\pm$1.5

facilitate co-registration with the transmission data, as CT images offer higher spatial resolution compared to the transmission scans, allowing clearer delineation of the inserts' boundaries. The protocol of the PCCT scan was not relevant for this study, as it was used only for registration purposes.

2.2 Methods

2.2.1 Linear attenuation coefficients (μ) derived from transmission measurements

The Sun Nuclear electron density phantom was scanned for one and a half hours using transmission scans on the ECAT EXACT HR + scanner. Since the removable head section could accommodate only ten inserts, the scans were divided into two separate sets (Set 1 and Set 2) to enable a total of fifteen inserts to be utilised. The high-density tissue replacement rod inserts (e.g., bone-equivalent materials) were uniformly distributed throughout the phantom to reduce reconstruction artefacts. To keep the phantom completely assembled during scanning, the remaining cavities were filled with additional non-target inserts. The configurations of sets 1 and 2 are illustrated in Figure 1. The transmission scan exhibited a true coincidence count rate of approximately 40.9 kcps, with a corresponding random count rate of 0.49 kcps and a singles rate of 2.33 Mcps, which together with the long scan time, lead to a transmission data set with very low variance. Additional scans of the same sets were conducted with the PCCT scanner.

The DIAGNOMATIC Pro-RT ED phantom was also scanned for a duration of 2 hours, utilising the same transmission protocol as on the ECAT EXACT HR + scanner. Due to the capacity limitation of the removable head section, which accommodates only nine inserts, all inserts were included in a single scan, except for the water-filled insert, as shown in Figure 2. The transmission scan exhibited a true coincidence count rate of approximately 154.7 kcps, with a corresponding random count rate of 7.3 kcps and a singles rate of 9.7 Mcps. An additional scan of the same set was performed using the PCCT scanner.

2.2.2 Linear attenuation coefficients (μ) for tissue-equivalent inserts

To determine the theoretical LACs at 511, 603, 1077, and 1157 keV for the phantom inserts, the XCOM database provided by the National Institute of Standards and Technology (NIST) was utilised. This database provides calculated cross-sections for elemental interactions for any composition. The calculations were completed using the chemical compositions provided in the data sheets of the Sun Nuclear electron density

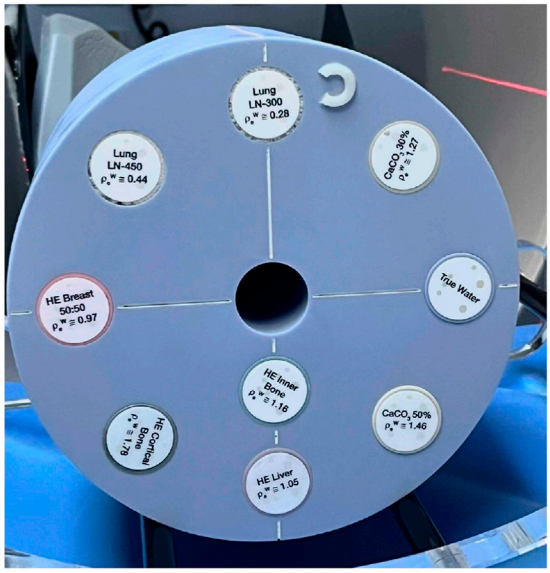

a

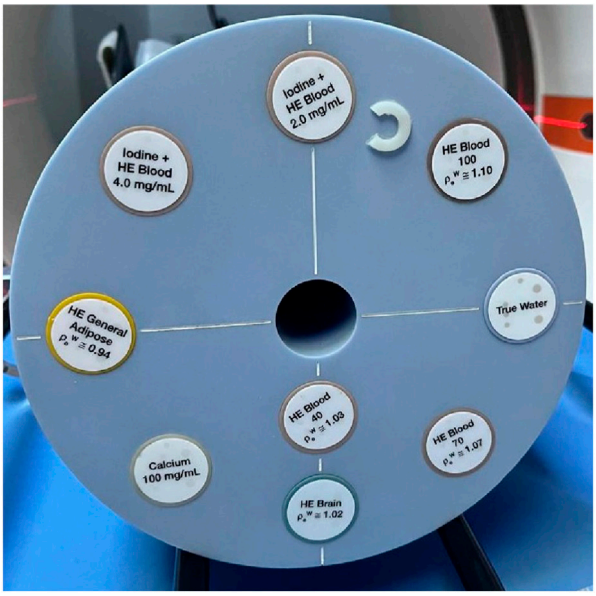

b

FIGURE 1
Insert layouts for Set 1 and Set 2 in the Sun Nuclear electron density phantom. For Set 1, the inserts—arranged clockwise starting from the top—are: lung LN-300, 30% $CaCO_3$, true water, 50% $CaCO_3$, liver, cortical bone, breast, lung LN-450, and inner bone. For Set 2, the inserts—also arranged clockwise from the top—are: blood + iodine 2 mg/mL, HE blood 100, true water, HE blood 70, brain, calcium 100 mg/mL, adipose, blood + iodine 4 mg/mL, and HE blood 40. *Not* all of the inserts shown were used in this study, i.e., the inserts 30% $CaCO_3$, true water, and calcium 100 mg/mL were only included in the phantom during CT scanning to avoid potential image artefacts caused by large air cavities. The inserts included in this study are listed in Table 1. **(a)** Set 1. **(b)** Set 2.

phantom inserts. However, the chemical compositions of the DIAGNOMATIC Pro-RT ED phantom inserts were not available; therefore, equivalent calculations for this phantom were not performed.

FIGURE 2
Insert layouts for the DIAGNOMATIC Pro-RT ED phantom. The inserts—arranged clockwise starting from the top—are lung (inhale), solid trabecular bone 200 mg/cc HA, solid dense bone 800 mg/cc HA, liver, solid dense bone 1250 mg/cc HA, breast, adipose, lung (exhale), and muscle.

2.2.3 Linear attenuation coefficients (μ) of literature values of real tissues corresponding to phantom inserts

The XCOM database was also used to determine the LACs at 511, 603, 1077, and 1157 keV for the literature values of real tissues corresponding to the phantoms' inserts. Instead of using the insert compositions themselves, the compositions of the corresponding literature values of real tissues represented by each insert were applied. Table 3 shows the chemical compositions and mass density (ρ) of the selected body tissues.

For the Sun Nuclear electron density phantom, the inserts labelled lung LN-300 and lung LN-450 were associated with inhaled and exhaled lung tissue, respectively, based on a comparison of their chemical compositions and physical density. In the DIAGNOMATIC Pro-RT ED phantom, the inserts labelled solid dense bone 1250 mg/cc HA, solid dense bone 800 mg/cc HA, and solid trabecular bone 200 mg/cc HA were associated with cortical bone, rib bone, and inner bone (spongiosa), respectively. These associations were established through a comparison of their attenuation coefficients with those of the corresponding bone tissues.

The literature values of real chemical compositions of all inserts and their mass density were identified based on the data provided in

TABLE 3 Chemical composition and mass density (ρ) of the corresponding body tissues as reported in the ICRU report 44.

Tissue	H	C	N	O	Others	ρ (g/cm^3)
Lung	10.3	10.5	3.1	74.9	0.2 Na, 0.2 P, 0.3 S, 0.3 Cl, 0.2 K	0.5 (deflated), 0.26 (inflated)
Liver	10.2	13.9	3.0	71.6	0.2 Na, 0.3 P, 0.3 S, 0.2 Cl, 0.3 K	1.06
Rib[a]	3.4	15.5	4.2	43.5	0.1 Na, 0.2 Mg, 10.3 P, 0.3 S, 22.5 Ca	1.92
Skull[a]	5.0	21.2	4.0	43.5	0.1 Na, 0.2 Mg, 8.1 P, 0.3 S, 17.6 Ca	1.61
Brain	10.7	14.5	2.2	71.2	0.2 Na, 0.4 P, 0.2 S, 0.3 Cl, 0.3 K	1.04
Breast	10.6	33.2	3.0	52.7	0.1 Na, 0.1 P, 0.2 S, 0.1 Cl	1.02
Muscle	10.2	14.3	3.4	71.0	0.1 Na, 0.2 P, 0.3 S, 0.1 Cl, 0.4 K	1.05
Adipose	11.4	59.8	0.7	27.8	0.1 Na, 0.1 S, 0.1 Cl	0.95
Inner bone	8.5	40.4	2.8	36.7	0.1 Na, 0.1 Mg, 3.4 P, 0.2 S, 0.2 Cl, 0.1 K, 7.4 Ca, 0.1 Fe	1.18
Cortical bone	3.4	15.5	4.2	43.5	0.1 Na, 0.2 Mg, 10.3 P, 0.3 S, 22.5 Ca	1.92
Blood	10.2	11.0	3.3	74.5	0.1 Na, 0.1 P, 0.2 S, 0.3 Cl, 0.2 K, 0.1 Fe	1.06
Blood + Iodine 2 mg/ml[b]	10.2	11.0	3.3	74.3	0.1 Na, 0.1 P, 0.2 S, 0.3 Cl, 0.2 K, 0.1 Fe, 0.20 I	1.06
Blood + Iodine 4 mg/ml[b]	10.12	11.0	3.3	74.2	0.1 Na, 0.1 P, 0.2 S, 0.3 Cl, 0.2 K, 0.1 Fe, 0.38 I	1.06

[a]The chemical composition and mass density (ρ) of the skull and rib were found in Boersma (2021).
[b]The chemical compositions and mass densities (ρ) of the Blood + Iodine inserts were computed as described in 2.2.3.
These compositions are referred to as *literature values*throughout the manuscript.

ICRU 44, except for the insert with 50% $CaCO_3$ of the Sun Nuclear electron density phantom and the solid dense bone 800 mg/cc HA insert in the DIAGNOMATIC Pro-RT ED phantom. These two inserts were associated with skull and rib bone compositions, respectively; their chemical compositions and mass density were obtained from [33], based on a comparison of their attenuation coefficients with those of skull and rib bones. The attenuation values were found to be in close agreement. Other inserts were directly identified by their names.

The HE Blood 40 insert was associated with the composition of normal blood, as reported in ICRU 44, based on its chemical composition and identical physical density, as confirmed by the blood density value provided in [34]. The HE Blood 70 and the HE Blood 100 inserts were associated with blood containing higher haemoglobin concentrations, since higher haemoglobin levels correspond to increased CT values [35, 36]. This is reflected in the phantom data sheet, where both Blood 70 and Blood 100 have higher CT values. However, the chemical composition of blood with higher haemoglobin could not be found, and thus, the LACs for literature values of real tissues could not be determined.

For the inserts containing blood with iodine, the chemical compositions were estimated by accounting for the effect of iodine on the overall chemical composition. This estimation was done by assuming a blood density of 1.06 mg/mL and a reference blood volume of 5000 mL, and first calculating the iodine percentage in the blood, followed by determining the total mass of the blood and the mass percentage of iodine. The chemical compositions of blood were then adjusted accordingly to incorporate the iodine contribution.

2.3 Data analysis

Amide software (version 1.0.6) was used to co-register the ECAT data and the corresponding CT images and to extract LACs at 511 keV. Three fiducial marks were placed separately on the phantoms for both the transmission and PCCT scans to allow exact alignment. Cylindrical regions of interest (ROIs) were defined with a diameter of 10 mm and a length of 10 mm, positioned centrally within each insert. The spatial resolution of the ECAT EXACT HR + scanner is 7.4 mm in the worst case, at an offset of 100 mm from the iso-center [37]. Bearing in mind the diameter of the inserts (28.6 mm), the inserts were modeled as a 2D boxcar function of width 28.6 mm and convolved with a 2D Gaussian point spread function (PSF) with a full width at half maximum (FWHM) of 7.4 mm (and corresponding standard deviation σ = FWHM/2.35) representing the scanner's spatial resolution. With this estimation, the amplitude within the extension of the ROI with a diameter of 1 cm was (0.9997) of the true value, indicating that PVE can be neglected. Finally, the LACs at 511 keV were extracted from the ROIs for each insert using the ROI statistics tools in Amide. The ROIs in both the PCCT and ECAT transmission scans in Amide software are shown in Figure 3.

The standard error (SE) of the measured insert LACs was calculated in the common way, i.e., SE = $\sigma/\sqrt{N}$, where σ is the standard deviation and N is the number of voxels that were extracted using the Amide software.

To evaluate the consistency between the measured LACs of the insert and the corresponding LACs obtained via X-com of the Sun Nuclear electron density phantom, we calculated the z-score (assuming a measurement uncertainty of 2%). We also calculated the probability of each measurement being compatible with the LAC values obtained from the insert compositions.

As the chemical compositions of the DIAGNOMATIC Pro-RT ED phantom are not provided, computation of corresponding XCOM LACs was not possible. Only a comparison of measurements with the XCOM values for the literature values of real tissue compositions that are represented by the inserts was possible. In

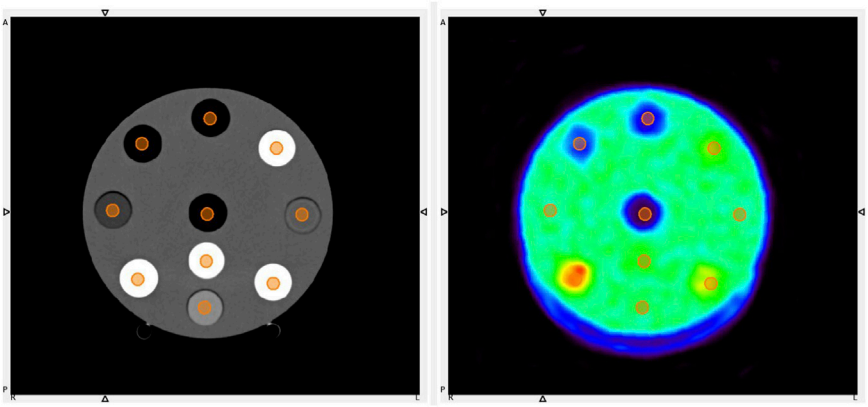

FIGURE 3
Cylindrical regions of interest (ROIs) with a diameter of 10 mm and a length of 10 mm, positioned centrally within each insert, in both the PCCT and ECAT transmission scans. (The bluish arc below the phantom in the transmission image is from the head holder).

contrast, for the sun nuclear phantom, comparisons between XCOM values for the insert compositions and measurements were also possible; these comparisons indicated detailed information on the level of confidence of the measurements.

The total attenuation coefficients at 511, 603, 1077, and 1157 keV were calculated using the NIST XCOM database, based on the chemical compositions of either the literature values of real tissue or the tissue-equivalent inserts. The total attenuation values with coherent scattering were selected. These coefficients were subsequently multiplied by the corresponding physical densities of the literature values of real tissues or inserts to obtain the LACs.

3 Results

Table 4 together with Figure 4, shows the LACs at 511 keV for the tissue-equivalent insert compositions obtained via XCOM, the corresponding measured LACs of these inserts, and the corresponding LACs obtained via XCOM for the literature values of real tissue compositions for the Sun Nuclear electron density phantom. Measurement values were given with the statistical measurement error (standard error of the mean), excluding systematic errors potentially due to scattered radiation and other effects. The LACs derived from the literature values of real tissue compositions were used as reference values, as the phantom inserts were designed to mimic real tissues; therefore, the literature values of real tissue compositions were considered the ground truth. Relative differences were then calculated by comparing these reference values with both the measured LACs of the inserts and those of the tissue-equivalent insert compositions. For the phantom where the tissue-equivalent insert compositions were known, the relative differences between LACs of the tissue-equivalent insert compositions and the measured LACs of the inserts were also computed. The relative differences between the measured LACs and LACs derived from literature values of real tissue compositions were within ±5% for all inserts, except for lung LN-300, 50% $CaCO_3$, iodine + HE Blood 2 mg/mL, iodine + HE Blood 4 mg/mL, and breast. The relative differences between LACs derived from insert compositions and literature values of real tissue compositions were within ±5% for all inserts, except for the lung tissue equivalent inserts. The lung-equivalent inserts show high deviations, with 8% for lung inhale and 12% for lung exhale when comparing XCOM-derived LACs for insert compositions and literature values of real tissue compositions. When comparing LACs from the measured insert with the literature values of real tissue compositions, the lung inhale insert deviation is even larger, reaching 37%, whereas the lung exhale insert shows an almost negligible deviation. Also, the lung-equivalent inserts show high deviations, with 26% for lung inhale and 14% for lung exhale when comparing XCOM-derived LACs for insert compositions with the measured insert. The statistical measurement error is at least two orders of magnitude smaller than the observed differences between measured LACs and LACs from literature values of real tissue compositions. No consistent trend was observed, irrespective of whether the literature values of real tissue compositions LACs exceeded or fell below the insert compositions or the measured ones. Also, the results of the statistical comparison between the measured insert LACs and corresponding insert composition LACs of the Sun Nuclear electron density phantom are given in Table 4. Most soft-tissue inserts, including liver, brain, and breast, exhibited z-scores below threshold 1.96, indicating thus good agreement with the insert composition LACs within the 95% confidence interval. In contrast, adipose, lung inserts, and iodine-containing inserts showed z-scores above this threshold.

Table 5 together with Figure 5, shows the measured LACs at 511 keV and the corresponding LACs obtained via XCOM for literature values of real tissue compositions (reference values) for the DIAGNOMATIC Pro-RT ED phantom. The relative differences were also computed. It can be seen that the relative difference is within ±5% for only three inserts (liver, breast, and solid trabecular bone 200 mg/cc HA) when comparing the LACs of the literature values of real tissue compositions with the measured LACs. For the adipose insert, this difference is 8%, whereas for the lung inhale and exhale inserts, it reaches 21% and 32%, respectively. Relative differences of 26% can be observed for solid dense bone 800 mg/cc and 1250 mg/cc HA, respectively. Also, no consistent trend was observed, irrespective of whether the LACs of the literature values of real tissue compositions exceeded or fell below the measured ones. As in the case of the Sun

10.3389/fphy.2026.1819239

TABLE 4 Linear attenuation coefficients at 511 keV for insert compositions, measurements, and literature values of real tissue compositions (reference values), along with relative differences, z-score, and probability for the Sun Nuclear electron density phantom.

Inserts	Insert compositior LACs (1/*cm*)from XCOM	Measured insert LACs ±standard error (1/*cm*)	Literature values of real tissue compositior LACs (1/*cm*)from XCOM	Relative difference between LACs by literature values of real tissue compositior and insert compositior (%)	Relative difference between LACs by literature values of real tissue compositior and measured insert (%)	Relative difference between LACs by insert compositior and measured insert (%)	z-score	Probability
Liver	0.10087	0.10136 ±0.00013	0.10081	0.06	0.55	0.49	0.242	0.809
Brain	0.09805	0.09515 ±0.00011	0.09934	−1.30	−4.22	−2.96	1.524	0.128
Breast	0.09254	0.09003 ±0.00013	0.09734	−4.93	−7.51	−2.71	1.394	0.163
Adipose	0.09085	0.09470 ±0.00011	0.09127	−0.46	3.76	4.24	2.033	0.042
Lung LN-300	0.02686	0.03402 ±0.00009	0.02475	8.53	37.45	26.66	10.523	< 0.001
Lung LN-450	0.04168	0.04770 ±0.00015	0.04760	−12.44	0.21	14.44	6.310	< 0.001
Inner bone	0.11122	0.10829 ±0.00011	0.11050	0.65	−2.00	−2.63	1.353	0.176
50% $CaCO_3$	0.14052	0.13830 ±0.00024	0.14606	−3.79	−5.31	−1.58	0.803	0.422
Cortical bone	0.17119	0.16867 ±0.00011	0.17165	−0.27	−1.74	−1.47	0.747	0.455
HE blood 40	0.09911	0.09874 ±0.00017	0.10082	−1.70	−2.06	−0.37	0.187	0.851
HE blood 70	0.10244	0.10516 ±0.00017	NA[a]	2.66[a]	2.66[a]	2.66	1.293	0.196
HE blood 100	0.10578	0.10277 ±0.00013	NA[a]	- 2.85[a]	- 2.85[a]	−2.85	1.464	0.143
Iodine + HE blood 2 mg/ml[b]	0.09921	0.09550 ±0.00020	0.10101	−1.78	−5.45	−3.74	1.942	0.052
Iodine + HE blood 4 mg/ml[b]	0.09939	0.09446 ±0.00011	0.10119	−1.78	−6.65	−4.96	2.610	0.009

[a]The chemical compositions of blood with higher hemoglobin could not be found; therefore, their LACs, could not be determined, and the relative differences were calculated for those inserts between the insert composition (reference value) and measured insert.

[b]The literature values of real chemical compositions and the mass densities (ρ)of the Blood + Iodine inserts were computed as described in 2.2.3.

Nuclear electron density phantom, the statistical measurement error is at least two orders of magnitude smaller than the observed differences between measured LACs and LACs from literature values of real tissue compositions.

When comparing the two phantoms, both showed high relative differences for the lung inserts, with the aforementioned exception of the lung LN-450; however, only the DIAGNOMATIC Pro-RT ED phantom had substantial deviations for the high-density

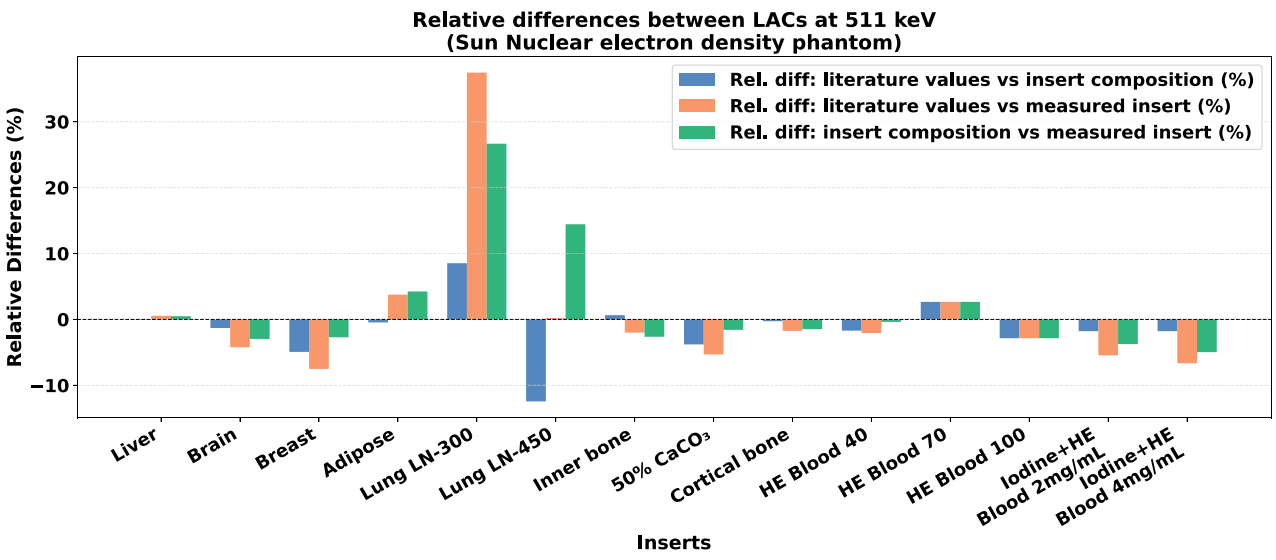

FIGURE 4
Relative differences between linear attenuation coefficients at 511 keV for insert compositions, measurements, and literature values of real tissue compositions (reference values) for the Sun Nuclear electron density phantom.

TABLE 5 **Linear attenuation coefficients at 511 keV for measurements and literature values of real tissue compositions (reference values), along with relative differences for the DIAGNOMATIC Pro-RT ED phantom.**

Inserts	Measured insert LACs ±standard error (1/*cm*)	Literature values of real tissue composition LACs (1/*cm*)from XCOM	Relative difference between LACs by literature values of real tissue composition and measured insert (%)
Liver	0.09998 ±0.00016	0.10081	−0.82
Muscle	0.09448 ±0.00025	0.09987	−5.40
Breast	0.09325 ±0.00007	0.09734	−4.20
Adipose	0.09879 ±0.00019	0.09127	8.24
Lung (inhale)	0.01940 ±0.00011	0.02475	−21.62
Lung (exhale)	0.06308 ±0.00011	0.04760	32.52
Solid trabecular bone 200 mg/cc HA	0.11012 ±0.00020	0.11050	−0.34
Solid dense bone 800 mg/cc HA	0.12681 ±0.00019	0.17161	−26.10
Solid dense bone 1250 mg/cc HA	0.12719 ±0.00015	0.17165	−25.90

bone inserts and adipose. Overall, the Sun Nuclear electron density phantom demonstrated better performance than the Pro-RT ED phantom for most inserts. The only insert for which the DIAGNOMATIC Pro-RT ED phantom showed a smaller relative difference compared to the Sun Nuclear phantom was with the breast insert. No consistent trend was observed regarding whether the LACs at 511 keV of the literature values of real tissue compositions exceeded or fell below the measured values in either phantom, nor when comparing the two phantoms together.

Tables 6–8 show the LACs at 603, 1077, and 1157 keV respectively, for the tissue-equivalent insert compositions obtained via XCOM, and the corresponding LACs obtained via XCOM for the literature values of real tissue compositions for the Sun Nuclear electron density phantom. The LACs derived from the literature values of the real tissue compositions were used as reference values. Relative differences were then calculated by comparing these reference values with LACs of the tissue-equivalent insert compositions. The relative differences were within ±5% for all inserts, except for the lung tissue equivalent inserts. The lung-equivalent inserts show high deviations, with 8% for lung inhale and 12% for lung exhale. Notably, however, the relative differences between LACs calculated using literature values of real tissue compositions and those based on insert

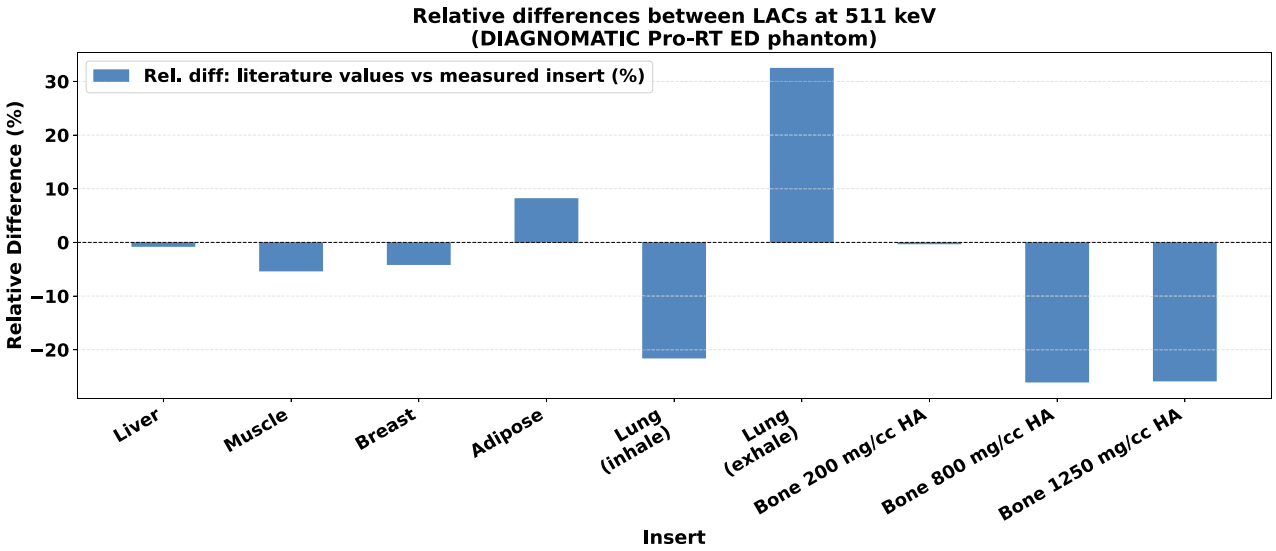

FIGURE 5
Relative differences between linear attenuation coefficients at 511 keV for measurements and literature values of real tissue compositions (reference values) for the DIAGNOMATIC Pro-RT ED phantom.

TABLE 6 **Linear attenuation coefficients at 603 keV for insert compositions and literature values of real tissue compositions (reference values), along with relative differences for the Sun Nuclear electron density phantom.**

Inserts	Insert composition LACs (1/*cm*)from XCOM	Literature values of real tissue composition LACs (1/*cm*)from XCOM	Relative difference between LACs by literature values of real tissue composition and insert composition (%)
Liver	0.09392	0.09385	0.07
Brain	0.09129	0.09249	−1.30
Breast	0.08616	0.09063	−4.93
Adipose	0.08460	0.08499	−0.46
Lung LN-300	0.02501	0.02304	8.55
Lung LN-450	0.03881	0.04432	−12.43
Inner bone	0.10353	0.10285	0.66
50% $CaCO_3$	0.13074	0.13588	−3.78
Cortical bone	0.15923	0.15963	−0.25
HE blood 40	0.09227	0.09386	−1.69
HE blood 70	0.09539	NA[a]	NA[a]
HE blood 100	0.09848	NA[a]	NA[a]
Iodine + HE blood 2 mg/ml[b]	0.09236	0.09403	−1.78
Iodine + HE blood 4 mg/ml[b]	0.09252	0.09419	−1.77

[a]The chemical compositions of blood with higher hemoglobin could not be found; therefore, their LACs, could not be determined, and the relative differences were not calculated for those inserts.
[b]The literature values of real chemical compositions and mass densities (ρ)of the Blood + Iodine inserts were computed as described in 2.2.3.

compositions were very similar across all investigated photon energies (511, 603, 1077, and 1157 keV) and exhibited the same sign for all inserts. However, this comparison could only be performed for the Sun Nuclear electron density phantom, as the chemical compositions of the DIAGNOMATIC Pro-RT ED phantom inserts were not available.

TABLE 7 Linear attenuation coefficients at 1077 keV for insert compositions and literature values for real tissue compositions (reference values), along with relative differences for the Sun Nuclear electron density phantom.

Inserts	Insert composition LACs ($1/cm$)from XCOM	Literature values of real tissue composition LACs ($1/cm$)from XCOM	Relative difference between LACs by literature values of real tissue composition and insert composition (%)
Liver	0.07167	0.07160	0.10
Brain	0.06967	0.07056	−1.26
Breast	0.06576	0.06916	−4.92
Adipose	0.06457	0.06486	−0.45
Lung LN-300	0.01908	0.01758	8.53
Lung LN-450	0.02961	0.03381	−12.42
Inner bone	0.07895	0.07843	0.66
50% $CaCO_3$	0.09962	0.10354	−3.79
Cortical bone	0.12124	0.12156	−0.26
HE blood 40	0.07042	0.07161	−1.66
HE blood 70	0.07278	NA[a]	NA[a]
HE blood 100	0.07516	NA[a]	NA[a]
Iodine + HE blood 2 mg/ml[b]	0.07046	0.07173	−1.77
Iodine + HE blood 4 mg/ml[b]	0.07057	0.07183	−1.75

[a]The chemical compositions of blood with higher hemoglobin could not be found; therefore, their LACs, could not be determined, and the relative differences were not calculated for those inserts.
[b]The literature values of real chemical compositions and mass densities (ρ)of the Blood + Iodine inserts were computed as described in 2.2.3.

4 Discussion

In this study, the accuracy of linear attenuation coefficients was evaluated at 511, 603, 1077, and 1157 keV for various tissue-equivalent inserts using two different commercial CT phantoms. Overall, the Sun Nuclear phantom demonstrated higher accuracy, with most inserts showing deviations within ± 5%. For the second phantom, only three out of nine inserts showed deviations from the reference values of less than ± 5%. Substantial deviations were observed in the lung-equivalent inserts for both phantoms. This can be attributed to the difficulty in accurately mimicking lung tissue, primarily due to its inherently non-uniform mechanical properties [38]. This is also supported by our findings, i.e., that the CT images of these compartments reveal the presence of numerous gaseous inclusions (as seen in Figure 6). While the number of the visible inclusions observed cannot account for the discrepancies between our measurements and the XCOM values, it is plausible that a substantial number of smaller gaseous inclusions remain unresolved by the CT system. Notably, the inserts in question appear significantly less homogeneous than other inserts, which show a better agreement between the measurements and XCOM-derived values, e.g., water and liver shown in Figure 6. Therefore, we infer that the XCOM values derived from these specific compositions fail to accurately reflect the true attenuation properties of the lung inserts. This discrepancy likely arises from the fact that the reported chemical composition pertains only to the solid component, overlooking the influence of gaseous inclusions. Moreover, the statistical comparison between the measured LACs of the inserts and the corresponding LACs from the insert compositions of the Sun Nuclear electron density phantom shows that most z-scores fall within the confidence interval of 95%. There are, however, a few exceptions: adipose, iodinated blood, and lung inserts. The high z-score values for the lung inserts indicate a significant mismatch between the measured LACs and those obtained with XCOM based on the insert compositions because of the explanation given above. The other three inserts (adipose and two inserts of iodine + HE blood) are close to the 5% threshold; however, as noted in the footnote of Table 4, there is additional uncertainty with the iodine + HE blood inserts because their compositions were estimated by us rather than being provided by the manufacturer. While a comparison between measurements and XCOM-derived LACs based on the inserts' composition was not possible for the Diagnomatic Pro-RT ED phantom, the Sun Nuclear electron density phantom demonstrates better agreement when comparing measured values to XCOM-derived LACs based on tissue composition, particularly for the bone compartments. Given that the insert sets of both phantoms are partially complementary, for future studies a combination of selected inserts from each phantom can be used to achieve a more complete and accurate set of tissue substitutes, with deviations maintained below 5%.

For the DIAGNOMATIC Pro-RT ED phantom, the values given in the names of the bone inserts (i.e. 200 mg/cc HA, 800 mg/cc HA, and 1250 mg/cc HA) most likely correspond to the HA content. The meaning of 'HA' was not specified in the product documentation,

TABLE 8 Linear attenuation coefficients at 1157 keV for insert compositions and literature values for real tissue compositions (reference values), along with relative differences for the Sun Nuclear electron density phantom.

Inserts	Insert composition LACs (1/*cm*)from XCOM	Literature values of real tissue composition LACs (1/*cm*)from XCOM	Relative difference between LACs by literature values of real tissue composition and insert composition (%)
Liver	0.06913	0.06908	0.07
Brain	0.06720	0.06808	−1.29
Breast	0.06344	0.06671	−4.90
Adipose	0.06228	0.06257	−0.46
Lung LN-300	0.01841	0.01696	8.55
Lung LN-450	0.02856	0.03262	−12.45
Inner bone	0.07615	0.07566	0.65
50% $CaCO_3$	0.09610	0.09987	−3.77
Cortical bone	0.11696	0.11725	−0.25
HE blood 40	0.06792	0.06908	−1.68
HE blood 70	0.07021	NA[a]	NA[a]
HE blood 100	0.07249	NA[a]	NA[a]
Iodine + HE blood 2 mg/ml[b]	0.06797	0.06919	−1.76
Iodine + HE blood 4 mg/ml[b]	0.06807	0.06929	−1.76

[a]The chemical compositions of blood with higher hemoglobin could not be found; therefore, their LACs, could not be determined, and the relative differences were not calculated for those inserts.
[b]The literature values of real chemical compositions and mass densities (ρ)of the Blood + Iodine inserts were computed as described in 2.2.3.

FIGURE 6
Close-ups of the CT images for lung, liver, and water inserts with adjusted gray-scales (linear). The lung inserts appear very inhomogeneous compared to the water and liver inserts.

but it potentially refers to hydroxyapatite. Noticeably, for the two solid dense bone inserts with 800 mg/cc HA and 1250 mg/cc HA, the measured LACs differ only by approximately 1%, while the corresponding insert mass densities (given in Table 2) differ by 10%, which can be explained by a potential compensation of the density-induced LAC-differences by material compositions with different electron densities. Unfortunately, as stated before, the material compositions of these inserts are not known.

As expected, LAC values decrease as photon energy increases due to the lower likelihood of interaction. The relative differences in XCOM values, based on the composition of the insert, remained consistent across all energies investigated. This suggests that variations are primarily driven by material composition and density, rather than energy-related effects. Furthermore, Compton scattering dominates attenuation in the scanned object at all examined energy levels. For nuclides that emit additional gamma photons with energies above 1022 keV, e.g., ^{44}Sc and ^{68}Ga, pair production can occur. However, the effect of pair production varies depending on photon energy and material properties and is not the dominant factor at the energies considered. The accuracy of our findings at these energies is comparable to that observed at 511 keV. This indicates that the presented approach is suitable for computing attenuation maps for higher gamma energies, which is essential for applications involving isotopes that emit additional prompt gammas [30].

The relationship between LACs and electron density is linear and exhibits high accuracy (as illustrated in Figure 7). This level of precision was unexpected, as existing transformation schemes, such

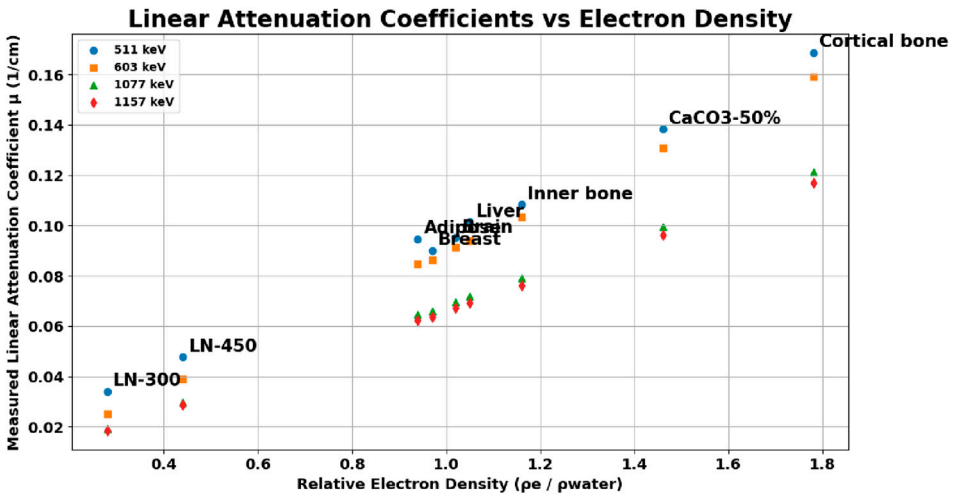

FIGURE 7
Measured linear attenuation coefficients vs. electron density values from the manufacturer. The electron density data for the three blood inserts and the two iodine-blood inserts are not provided in the data sheet; therefore, these inserts were excluded from the electron density plot.

TABLE 9 Ratio of linear attenuation coefficients and mass attenuation coefficients at 511 keV for lung and cortical bone inserts of the Sun Nuclear electron density phantom (LR means literature values).

Sun nuclear inserts	$\frac{(\mu/\rho)_{\text{inserts compositions}}}{(\mu/\rho)_{\text{LR of real tissue compositions}}}$	$\frac{\mu_{\text{inserts compositions}}}{\mu_{\text{LR of real tissue compositions}}}$	$\frac{(\mu/\rho)_{\text{measured values}}}{(\mu/\rho)_{\text{LR of real tissue compositions}}}$	$\frac{\mu_{\text{measured values}}}{\mu_{\text{LR of real tissue compositions}}}$
Lung LN-300	0.97	1.09	1.23	1.37
Lung LN-450	0.97	0.88	1.11	1.00
Cortical bone	0.99	1.00	0.98	0.98

TABLE 10 Ratio of linear attenuation coefficients and mass attenuation coefficients at 511 keV for muscle, lung, and bone inserts of the DIAGNOMATIC Pro-RT ED phantom (LR means literature values).

Pro-RT ED inserts	$\frac{(\mu/\rho)_{\text{measured values}}}{(\mu/\rho)_{\text{LR of real tissue compositons}}}$	$\frac{\mu_{\text{measured values}}}{\mu_{\text{LR of real tissue compositons}}}$
Muscle	0.94	0.95
Lung (inhale)	1.16	0.78
Lung (exhale)	0.99	1.33
Solid dense bone 1250 mg/cc HA	0.91	0.74

as the one from Carney et al. [1], typically require bi-linear functions to convert HUs to LACs. These methods often show significant deviations from linear behavior for soft tissues. In contrast, we anticipate that a conversion scheme from electron density to LAC values would present much smaller deviations for soft tissues.

Although the exact accuracy of the ECAT EXACT HR + scanner transmission scan could not be determined, it was shown that transmission scans using $^{68}Ge/^{68}Ga$ can achieve an accuracy of around 2% for scan times of approximately 15 min (see Table 4 in [39]). However, it is important to note that the accuracy of these scans depends heavily on the number of counts collected [40, 41]. Under optimal conditions, an accuracy of 1% might be attainable (see Table 3.4 in [40]). In the measurements conducted here, the LAC for a water insert was evaluated and compared to the calculated value. The measured LAC was found to be $0.09415 \pm 0.00014\ (1/cm)$, while the computation using the NIST XCOM database produced a value of $0.09598\ (1/cm)$. This led to a relative difference of −1.91%, supporting the uncertainty range of 1%–2%. The 1%–2% accuracy limit of transmission scan-derived LACs can mainly be attributed to residual scatter contamination during transmission scanning, even when septa are used and scatter is corrected during reconstruction.

To facilitate a direct comparison with the findings of Singh et al. [15], we calculated the ratios of the LACs and mass attenuation coefficients of the insert compositions against literature values for real tissue compositions at 511 keV. We also calculated the ratios of the LACs and the mass attenuation coefficients obtained from the measurements against the literature values of real tissue compositions for several inserts from both phantoms. In terms of the mass attenuation coefficient, depending on the tissue substitutes studied, Singh et al. reported ratios between 0.99 and 1.04 for muscle tissue substitutes, 0.95 and 1.05 for cortical bone tissue substitutes, and 0.97 for lung tissue substitutes. However, these rather good agreements were not observed in our study (Tables 9, 10; Figures 8, 9). We noted significant inconsistencies in the ratios of mass attenuation and linear attenuation coefficients, particularly for lung inserts. As discussed above, this observation can be attributed to the inaccurate composition of the lung inserts, i.e.,

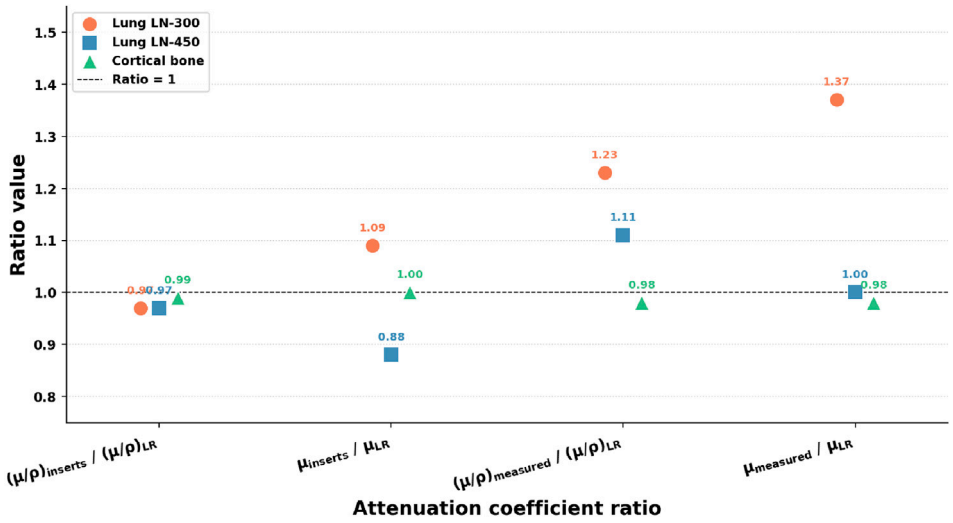

FIGURE 8
Ratio of linear attenuation coefficients and mass attenuation coefficients at 511 keV for lung and cortical bone inserts of the Sun Nuclear electron density phantom (LR means literature values).

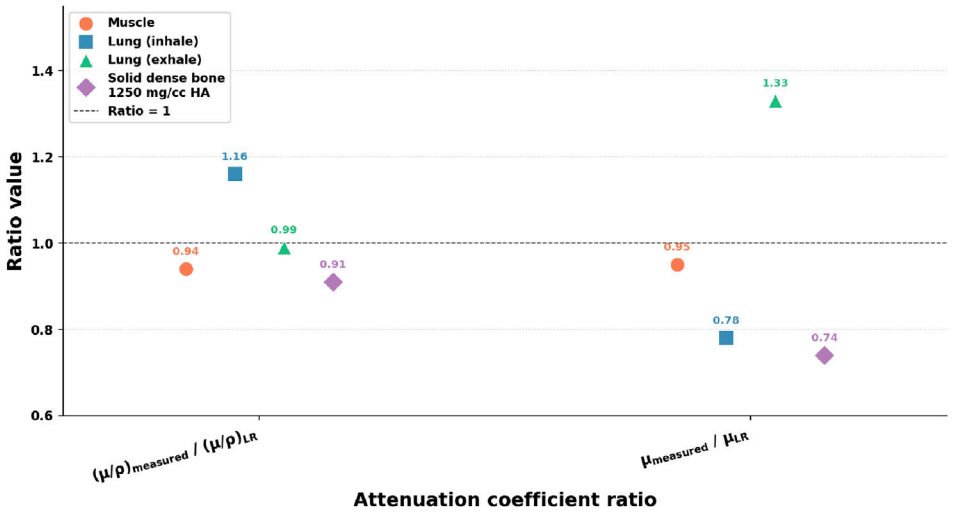

FIGURE 9
Ratio of linear attenuation coefficients and mass attenuation coefficients at 511 keV for muscle, lung, and bone inserts of the DIAGNOMATIC Pro-RT ED phantom (LR means literature values).

the missing gaseous phase volume and composition, as these parameters significantly impact the material density. Consistent values were observed for the muscle insert of the Pro-RT phantom and the cortical bone insert of the Sun Nuclear phantom. This finding suggests that lung phantom inserts could be developed that accurately simulate the attenuation properties of lung tissue for both CT and PET energies by adjusting the gas composition.

Similarly, White (1978) studied the ratios of mass attenuation coefficients between tissue substitutes and corresponding tissues at different energy levels between 10 and 100000 keV to determine which substitute most closely replicates radiation response. At energies of 100and 1000keV, White reported ratios between 0.99 and 1.04 for muscle tissue substitutes (including Goodman liquid, Rossi liquid, Harris wax, and paraffin wax), between 0.98 and 1.08 for cortical bone tissue substitutes (Caeron wax, Facey liquid, and plaster of paris), and between 0.96 and 0.98 for lung tissue substitutes (gelatine). These values are in good agreement with those obtained by Singh et al. [15]. However, upon comparing the chemical compositions of the Sun Nuclear electron density phantom inserts to those used by White, we found no suitable matches. The closest approximation was the substitute SB3 for cortical bone, although the element abundances were not identical. Furthermore, the chemical compositions of the real tissue examined by White (adipose, cortical bone, lung, and muscle) do not align perfectly

with those used in the present study; this discrepancy is expected, as White's work drew from older versions of Report 44, including ICRP Report 23 [42] and ICRU Report 10b [43].

Ermis et al. compared mass attenuation obtained from Monte Carlo simulations (using FLUKA and GEANT4) with XCOM values [18]. They observed good agreement between all three methods for various tissue compositions at PET energies (511 keV and above). However, at CT-like energies (especially 60 and 80 keV), they recorded differences of up to 25% for most of the tissues. Amin et al. evaluated the difference between the mass attenuation coefficients of soft-tissue and bone tissue substitutes by comparing experimental values with those calculated using XCOM [26]. They found that the differences were within the 5% interval for energies between 662 keV and 1.3 MeV for both tissue types.

The careful evaluation of systematic errors in LACs is essential because errors in LACs propagate into errors in the reconstructed PET images, primarily due to the necessary attenuation correction. As demonstrated by Abella et al. [44] (in Figure 8), there is an approximately proportional relationship between LAC errors and SUV_{max}, with a proportionality factor close to 1. This means that a ± x% error in LAC results in an approximately ± x% bias in SUVmax. Therefore, the LAC deviations reported in this work would likely induce SUV biases of a similar order. While these differences are unlikely to affect routine clinical image interpretation significantly, they may be relevant in quantitative research applications, such as neuroreceptor binding studies and functional activation studies, where even small systematic biases can impact the reliability and comparability of non-SUV-based quantitation.

This study has the following limitations: the data were acquired using only a single scanner. No *in vivo* validation was performed.

5 Conclusion

This study evaluated the accuracy of linear attenuation coefficients at 511, 603, 1077, and 1157 keV across various tissue-equivalent materials using the Sun Nuclear electron density phantom and the DIAGNOMATIC Pro-RT ED phantom. Twelve out of 23 tissue substitutes exhibited LAC deviations of less than 5% when compared to values from the NIST XCOM database. The largest errors were in lung-equivalent inserts, particularly the Sun Nuclear lung LN-300, which had a deviation of 37.45%, likely due to incomplete composition data. Additionally, solid dense bone inserts in the DIAGNOMATIC Pro-RT ED phantom showed significant deviations of about 26%. While deviations for most tissue substitutes in the Sun Nuclear phantom were smaller than 5%, lung inserts were exceptions. Combining specific inserts from both phantoms provides a set of tissue substitutes that reproduce attenuation at 511 keV and the other energies with systematic errors below 5%.

Data availability statement

The raw data supporting the conclusions of this article will be made available by the authors, without undue reservation.

Author contributions

HA: Conceptualization, Data curation, Formal Analysis, Funding acquisition, Investigation, Methodology, Project administration, Resources, Software, Supervision, Validation, Visualization, Writing – original draft, Writing – review and editing. LT: Data curation, Investigation, Software, Writing – review and editing. ON: Conceptualization, Investigation, Resources, Writing – review and editing. MZ: Investigation, Writing – review and editing. SS: Investigation, Writing – review and editing. OW: Investigation, Writing – review and editing. SF: Conceptualization, Investigation, Resources, Writing – review and editing. AA: Supervision, Writing – review and editing. MW: Conceptualization, Resources, Writing – review and editing. NS: Supervision, Writing – review and editing. CL: Conceptualization, Data curation, Formal Analysis, Funding acquisition, Investigation, Methodology, Project administration, Resources, Software, Supervision, Validation, Visualization, Writing – review and editing.

Funding

The author(s) declared that financial support was received for this work and/or its publication. This work is funded by the Palestinian-German Science Bridge (PGSB), the RETIMAGER project (Real Time Molecular Imager with Unsurpassed Resolution), and the Innovation Go fund by Forschungszentrum Jülich.

Conflict of interest

Author SF was employed by Department of Computed Tomography, Siemens Healthineers AG.

The remaining author(s) declared that this work was conducted in the absence of any commercial or financial relationships that could be construed as a potential conflict of interest.

Generative AI statement

The author(s) declared that generative AI was not used in the creation of this manuscript.

Any alternative text (alt text) provided alongside figures in this article has been generated by Frontiers with the support of artificial intelligence and reasonable efforts have been made to ensure accuracy, including review by the authors wherever possible. If you identify any issues, please contact us.

Publisher's note

All claims expressed in this article are solely those of the authors and do not necessarily represent those of their affiliated organizations, or those of the publisher, the editors and the reviewers. Any product that may be evaluated in this article, or claim that may be made by its manufacturer, is not guaranteed or endorsed by the publisher.

References

1. Carney JPJ, Townsend DW, Rappoport V, Bendriem B. Method for transforming CT images for attenuation correction in PET/CT imaging. *Med Phys* (2006) 33:976–83. doi: 10.1118/1.2174132

2. Kops ER, Alrakh H, Brambilla CR, Scheins J, Herzog H, Shah NJ, et al. Attenuation correction of the cerebellum in PET/MR data. *IEEE Trans Radiat Plasma Med Sci* (2024) 8:618–31. doi: 10.1109/TRPMS.2024.3370252

3. Xia T, Alessio AM, Kinahan PE. Dual energy CT for attenuation correction with PET/CT: DECT attenuation correction for PET/CT. *Med Phys* (2013) 41:012501. doi: 10.1118/1.4828838

4. Sodickson AD, Keraliya A, Czakowski B, Primak A, Wortman J, Uyeda JW. Dual energy CT in clinical routine: how it works and how it adds value. *Emerg Radiol* (2021) 28:103–17. doi: 10.1007/s10140-020-01785-2

5. Ladefoged CN, Law I, Anazodo U, St Lawrence K, Izquierdo-Garcia D, Catana C, et al. A multi-centre evaluation of eleven clinically feasible brain PET/MRI attenuation correction techniques using a large cohort of patients. *NeuroImage* (2017) 147:346–59. doi: 10.1016/j.neuroimage.2016.12.010

6. Wagenknecht G, Kaiser HJ, Mottaghy FM, Herzog H. MRI for attenuation correction in PET: methods and challenges. *Magn Reson Mater Phys Biol Med* (2013) 26:99–113. doi: 10.1007/s10334-012-0353-4

7. Kops ER, Herzog H (2008). *Template Based Attenuation Correction for Pet in mr-pet Scanners* In: *2008 IEEE Nuclear Science Symposium Conference Record* 3786–9. doi: 10.1109/NSSMIC.2008.4774281

8. Lee JS. A review of deep-learning-based approaches for attenuation correction in positron emission tomography. *IEEE Trans Radiat Plasma Med Sci* (2021) 5:160–84. doi: 10.1109/TRPMS.2020.3009269

9. Aubrey J, Esfandiari N, Baracos VE, Buteau FA, Frenette J, Putman CT, et al. Measurement of skeletal muscle radiation attenuation and basis of its biological variation. *Acta Physiol* (2014) 210:489–97. doi: 10.1111/apha.12224

10. Maillane-Vanegas S, Agostinete RR, Lynch KR, Ito IH, Luiz-de-Marco R, Rodrigues-Junior MA, et al. Bone mineral density and sports participation. *J Clin Densitom* (2020) 23:294–302. doi: 10.1016/j.jocd.2018.05.041

11. Cherukuri L, Kinninger A, Birudaraju D, Lakshmanan S, Li D, Flores F, et al. Effect of body mass index on bone mineral density is age-specific. *Nutr Metab Cardiovasc Dis* (2021) 31:1767–73. doi: 10.1016/j.numecd.2021.02.027

12. Peters N, Kieslich A, Wohlfahrt P, Hofmann C, Richter C. *In vivo* assessment of tissue-specific radiological parameters with intra- and inter-patient variation using dual-energy computed tomography. *Radiother Oncol* (2022) 175:34–41. doi: 10.1016/j.radonc.2022.07.021

13. Yang NC, Leichner PK, Hawkins WG. Effective atomic numbers for low-energy total photon interactions in human tissues. *Med Phys* (1987) 14:759–66. doi: 10.1118/1.596000

14. International Commission on Radiation Units and Measurements. Tissue substitutes in radiation dosimetry and measurement. *Tech Rep.* (1989).

15. Singh I, Singh B, Sandhu B, Sabharwal AD. Investigations of various gamma radiation interaction parameters of human tissues and their tissue substitute materials for dosimetric applications. *Radiat Phys Chem* (2021) 189:109742. doi: 10.1016/j.radphyschem.2021.109742

16. White DR. Tissue substitutes in experimental radiation physics. *Med Phys* (1978) 5:467–79. doi: 10.1118/1.594456

17. Berger M, Hubbell J, Seltzer S, Coursey J, Zucker D. *XCOM: Photon Cross Section Database* (1999).

18. Ermis EE, Pilicer FB, Pilicer E, Celiktas C. A comprehensive study for mass attenuation coefficients of different parts of the human body through monte carlo methods. *Nucl Sci Tech* (2016) 27:54. doi: 10.1007/s41365-016-0053-2

19. Frimaio A, Nascimento BC, Barrio RM, Campos LL, Costa PR. X-ray spectrometry applied for determination of linear attenuation coefficient of tissue-equivalent materials. *Radiat Phys Chem* (2019) 160:89–95. doi: 10.1016/j.radphyschem.2019.03.021

20. Nascimento BC, Frimaio A, Barrio RM, Sirico AC, Costa PR. Comparative analysis of the transmission properties of tissue equivalent materials. *Radiat Phys Chem* (2020) 167:108300. doi: 10.1016/j.radphyschem.2019.04.050

21. Kabir NA, Okoh FO, Mohd Yusof MF. Radiological and physical properties of tissue equivalent mammography phantom: characterization and analysis methods. *Radiat Phys Chem* (2021) 180:109271. doi: 10.1016/j.radphyschem.2020.109271

22. Gokcekuyu Y, Ekinci F, Buyuksungur A, Guzel MS, Acici K, Asuroglu T. Comparison of X-Ray absorption in mandibular tissues and tissue-equivalent polymeric materials using PHITS monte carlo simulations. *Appl Sci* (2024) 14:10879. doi: 10.3390/app142310879

23. Geraldelli W, Tomal A, Poletti ME. Characterization of tissue-equivalent materials through measurements of the linear attenuation coefficient and scattering profiles obtained with polyenergetic beams. *IEEE Trans Nucl Sci* (2013) 60:566–71. doi: 10.1109/TNS.2013.2248382

24. Büyükyıldız M, Kaur P, Thakur S, Atlı R. Study of phantom materials close to 1 keV photon energy for radiation applications. *Radiat Phys Chem* (2024) 215:111375. doi: 10.1016/j.radphyschem.2023.111375

25. Levet A, Thakur S, Kaur P, Rafiei MM, Parsaei S, Büyükyıldız M. Investigation of radiological properties and water equivalence of polymer gel dosimeters in the energy range 0.1–10 keV. *Nucl Eng Technology* (2025) 57:103387. doi: 10.1016/j.net.2024.103387

26. Amin NAB, Zukhi J, Kabir NA, Zainon R. Determination of effective atomic numbers from mass attenuation coefficients of tissue-equivalent materials in the energy range 60 keV-1.33 MeV. *J Phys Conf Ser* (2017) 851:012018. doi: 10.1088/1742-6596/851/1/012018

27. Soultanidis G, Herraiz JL, Fayad ZA, Grimm J, Teunissen AJP. Multiplexed imaging of radionuclides. *Nat Biomed Eng* (2025) 9:993–1006. doi: 10.1038/s41551-025-01406-8

28. Conti M, Eriksson L. Physics of pure and non-pure positron emitters for PET: a review and a discussion. *EJNMMI Phys* (2016) 3:8. doi: 10.1186/s40658-016-0144-5

29. Pratt EC, Lopez-Montes A, Volpe A, Crowley MJ, Carter LM, Mittal V, et al. Simultaneous quantitative imaging of two PET radiotracers via the detection of positron–electron annihilation and prompt gamma emissions. *Nat Biomed Eng* (2023) 7:1028–39. doi: 10.1038/s41551-023-01060-y

30. Pfaehler E, Niekämper D, Scheins J, Shah NJ, Lerche CW. ML-EM based dual tracer PET image reconstruction with inclusion of prompt gamma attenuation. *Phys Med & Biol* (2025) 70:015009. doi: 10.1088/1361-6560/ad9660

31. Adam LE, Zaers J, Ostertag H, Trojan H, Bellemann M, Brix G, et al. Performance evaluation of the whole-body pet scanner ecat exact hr/sup +. *1996 IEEE Nucl Sci Symp* (1996) 2:1270–4. doi: 10.1109/NSSMIC.1996.591677

32. Rajendran K, Petersilka M, Henning A, Shanblatt ER, Schmidt B, Flohr TG, et al. First clinical photon-counting detector CT system: Technical evaluation. *Radiology* (2022) 303:130–8. doi: 10.1148/radiol.212579

33. Boersma D. Gate/GateMaterials.db at develop· OpenGATE/Gate (2021). Available online at: https://github.com/OpenGATE/Gate/blob/develop/GateMaterials.db (Accessed April 8, 2021).

34. Ostadfar A. Biofluid mechanics: principles and applications. Academic Press (2016) 1–60. doi: 10.1016/B978-0-12-802408-9.00001-6

35. Schulz B, Euler A, Schmid HR, Kubik-Huch RA, Thali M, Niemann T. *In vitro* blood sample assessment: investigating correlation of laboratory hemoglobin and spectral properties of dual-energy CT measurements (ρ/Z). *Eur Radiol* (2024) 34:7934–43. doi: 10.1007/s00330-024-10820-6

36. Hagita T, Shiotani S, Toyama N, Tominaga N, Miyazaki H, Ogasawara N. Correlation between hounsfield unit values of blood in CT on immediate postmortem CT after cardiopulmonary resuscitation and antemortem hemoglobin levels. *Forensic Imaging* (2022) 30:200515. doi: 10.1016/j.fri.2022.200515

37. Grootoonk S, Newiger H, Byars L, Nutt R, Frackowiak R. Performance of the ECAT exact HR+ PET scanner in functional brain imaging. *NeuroImage* (1996) 3:S24. doi: 10.1016/S1053-8119(96)80026-7

38. Caro CG, Pedley TJ, Schroter RC, Seed WA, Parker KH. *The Pulmonary Circulation*. Cambridge University Press (1980). p. 467–506. doi: 10.1017/CBO9781139013406.018

39. Kinahan PE, Townsend DW, Beyer T, Sashin D. Attenuation correction for a combined 3D PET/CT scanner. *Med Phys* (1998) 25:2046–53. doi: 10.1118/1.598392

40. Yu SK. *Attenuation Correction in Positron Tomography*. Canada: McMaster University (1996).

41. Meikle SR, Dahlbom M, Cherry SR. Attenuation correction using count-limited transmission data in positron emission tomography. *J Nuclear Medicine* (1993) 34:143–50.

42. International Commission on Radiological Protection. *Report of the Task Group on Reference Man*, 23. Oxford, UK: International Commission on Radiological Protection (1975).

43. International Commission on Radiation Units and Measurements. *Physical Aspects of Irradiation: Recommendations of the Icru (Report 10b)*. Washington, D.C., USA: International Commission on Radiation Units and Measurements (1964).

44. Abella M, Alessio AM, Mankoff DA, MacDonald LR, Vaquero JJ, Desco M, et al. Accuracy of CT-based attenuation correction in PET/CT bone imaging. *Phys Med Biol* (2012) 57:2477–90. doi: 10.1088/0031-9155/57/9/2477